Journal Pre-proof

Exosome-based delivery of RNAi leads to breast cancer inhibition

Renata Silva, Débora Ferreira, Lígia R. Rodrigues

1   **Exosome-based delivery of RNAi leads to breast cancer inhibition**

2   **Renata Silva [1,2,+], Débora Ferreira [1,2,+] and Lígia R. Rodrigues [1,2*]**

3   [1]   CEB – Centre of Biological Engineering, University of Minho, 4710-057 Braga, Portugal

4   [2]   LABBELS – Associate Laboratory, Braga, Guimarães, Portugal

5   [*]   Correspondence: lrmr@deb.uminho.pt;

6   [+]   These authors contributed equally to this work

7

8   **Abstract**

9   Breast cancer is currently the most prevalent cancer in the world. It has been reported

10   that hyperactivation and dysregulation of key pathways, such as PI3K/AKT/mTOR

11   (PAM), contributes to the cell's tumorigenesis and resistance to existent therapies.

12   Herein, we sought to uncover the potential of PAM downregulation in a panel of different

13   breast cancer cell lines with different phenotypes, through *PIK3CA* silencing. This

14   oncogene was targeted with a pre-designed small interfering RNA (siRNA) transfected

15   onto *PIK3CA* wild-type MDA-MB-231 cells and *PIK3CA* mutated MDA-MB-453 cells. The

16   results suggest that the siRNA efficiently targeted *PIK3CA*, triggering an efficient gene

17   silencing and a decrease on cellular viability, as well as migration capacity. Moreover,

18   exosome-like nanovesicles were successfully isolated, characterized and incorporated

19   into the cells and served as excellent siRNA nanocarriers, promoting an incremented

20   and faster onset. Altogether, the data gathered shows that the combination of the

21   validated siRNA with these nanocarriers could be a promising targeted drug delivery

22   system for an alternative breast cancer therapy.

23   **Keywords:** Breast cancer; Drug delivery system; Exosomes

24

1. Introduction

Breast cancer is currently the most diagnosed cancer worldwide, surpassing lung cancer with 11.7% of all cancer cases. Although advances in cytotoxic chemotherapy and targeted strategies have allowed an improvement of the clinical scenario, breast cancer is still the leading cause of cancer related deaths in women [1]. Accounting for approximately 15% of breast cancer cases, triple negative breast cancer (TNBC) is defined by the lack of expression of estrogen, progesterone, and human epidermal growth factor 2 (HER2) receptors. TNBC aggressiveness and proliferative nature promotes poorer prognoses and low survival rates that are hampered by the paucity of successful therapies and the reduced number of effective therapeutic targets [2–4].

In the latest years, in order to overcome the poor clinical outcomes and resistance of existent therapies, several pathways have been identified as possible targets, including the PI3K/AKT/mTOR (PAM) cascade [5]. Such pathway is frequently over-activated and dysregulated in breast cancer cases, allowing cancer cells expansion, dissemination and malignancy transformation [6]. The major player in the PAM pathway is the phosphoinositide 3 kinase (PI3K) heterodimer, composed of a catalytic subunit p110 (p110α/PIK3CA, p110β/PIK3CB or p110δ/PIK3CD) that interacts with a regulatory subunit p85 (p85α, p55α, p50α, p85β or p55γ) [7]. Mutations in *PIK3CA* are the most common event in breast cancer, representing, in TNBC, the second most frequently mutated gene after tumor protein P53. The TNBC scenario is aggravated by inactivating alterations in *PTEN* and activating mutations in *AKT* [7,8].

The discovery and development of novel therapies profited from the discovery of RNA interference (RNAi) machinery in the gene silencing field, including the small interfering RNA (siRNA) and microRNA (miRNA) modalities, as a powerful tool for the knockdown of targeted genes [9]. Specifically, siRNA can trigger the expression inhibition of a certain target gene in a sequence-specific manner by mediating targeted mRNA degradation [10]. Moreover, such RNAi-based therapeutics exhibit innate advantages over small molecular drugs due to the execution of such function by complete Watson-Crick base pairing with mRNA, not requiring the recognition of protein spatial conformation. However, the application of siRNA as an unshielded molecule is compromised and requires the use of an effective delivery strategy [11,12].

Over the past decades, extracellular vesicles (EVs), in particular exosomes (30-150 nm) [13] have been subject of increasing attention due to a plethora of therapeutic and diagnostic applications, including its use as nanocarriers in drug delivery systems [14,15]. These molecules offer many advantages, such as small size, natural stability, biocompatibility, intercellular communication capacity and increased ability to escape from the immune system and degradation. Moreover, they possess an aqueous core that

62 allows the loading and protection of several classes of therapeutic molecules, including

63 siRNA, and also enable the cellular uptake mediated by recognition processes [14,16–

64 18].

65   In this study, we explored the implementation of an exosome-based siRNA targeting

66 *PIK3CA* delivery system for application in breast cancer therapy. The *PIK3CA*-targeting

67 siRNA (siPIK3CA) was tested against breast cancer cells using a lipofection-based

68 transfection approach. The effects on protein and mRNA expression, cellular viability

69 and migration were assessed and the interference of *PIK3CA* mutation was explored.

70 Next, the siPIK3CA was loaded onto BJ-derived exosomes (BJExo) using an optimized

71 electroporation approach. The cellular incorporation, as well as biological activity were

72 studied and further compared with the effect obtained using the conventional transfection

73 agent. We hypothesize that *PIK3CA* is a valid target for therapeutic intervention for

74 breast cancer and foresee that exosomes will allow a safe and effective siPIK3CA

75 delivery.

76

77 **2. Materials and Methods**

78

79   **2.1 Reagents**

80   4′,6-Diamidino-2-Phenylindole dihydrochloride (DAPI) was purchased from Biotium.

81 Lipofectamine RNAiMAX transfection reagent, 1,1'-Dioctadecyl- 3,3,3',3'-

82 Tetramethylindocarbocyanine Perchlorate (CM-DiI Dye) and Trizol were purchased from

83 Invitrogen. Alexa fluor 488-Phalloidin was acquired from Molecular Probes. Bovine

84 Serum Albumin (BSA) was purchased from Nzytech. 3-(4,5-Dimethylthiazol-2-yl)-2,5-

85 Diphenyltetrazolium Bromide (MTT) reagent, paraformaldehyde (PFA) and OptiPrep

86 density gradient medium were purchased from Sigma Aldrich. Sodium dodecyl sulfate

87 (SDS), dimethyl sulfoxide (DMSO) and propidium iodide (PI) were obtained from Thermo

88 Fisher Scientific.

89

90   **2.2 Cell lines and culture conditions**

91   Human breast cancer cell lines MDA-MB-231 (ATCC HTB-26) and MDA-MB-453

92 (ATCC HTB-131) were grown on tissue culture treated flasks in Dulbecco's Modified

93 Eagle Medium (DMEM, Biochrom) supplemented with 10% Fetal Bovine Serum (FBS,

94 Biochrom) and 1% Zell-shield antibiotic (Minerva Biolabs). The human fibroblast BJ cell

95 line (ATCC CRL-2522) was cultured in a 4:1 proportion of DMEM: Medium 199 (PAN-

96 Biotech), supplemented with 10% (v/v) FBS, 1% (v/v) antibiotic and 0,01% (v/v)

97   hygromycin B (Sigma Aldrich). All cells were authenticated, checked for mycoplasma

98   contamination and maintained at 37°C and a 5% CO_2 humid atmosphere.

99

100   **2.3 Lipofectamine-based siRNA delivery**

101   2.3.1 siRNA transfection

102   Transient knockdown was achieved using a pre-designed *PIK3CA*-targeting siRNA

103   (siPIK3CA: 5'- UUCGCACCACCUCAAUAAG-3') from Sigma Aldrich and a non-targeting

104   siRNA (siNC) that does not interact with any sequences in the human transcriptome

105   provided by Integrated DNA Technologies. Cells were seeded at a 50-60% confluency

106   in a 6 well-plate and incubated at 37°C, 24 h before siPIK3CA transfection. Then, cells

107   were washed with PBS 1× and incubated with serum-free DMEM. The siRNAs (25 or 50

108   nM) and Lipofectamine RNAiMAX were pre-diluted in Opti-MEM (reduced serum

109   medium, Gibco). Both were pre-mixed for about 20 min at room temperature, allowing

110   the complexes' formation, before being added to the cells. The transfection mixture was

111   removed after 24 h and cell culture medium was added to the wells.

112

113   2.3.2 Assessment of protein expression by western blotting

114   Protein was extracted from cells using the radioimmunoprecipitation assay (RIPA)

115   buffer supplemented with a proteinase inhibitor cocktail. The cellular protein

116   concentration was determined by Pierce BCA Protein Assay Kit (Thermo Fisher

117   Scientific) and 20 µg of total protein were loaded, separated in 10 or 15%

118   polyacrylamide/SDS gel electrophoresis and transferred onto methanol activated PVDF

119   membranes (Macherey-Nagel). The membranes were blocked for 1 h with 5% non-fat

120   milk in Tris-buffered saline (TBS) supplemented with 0.1% Tween 20 and then

121   immunoblotted with primary antibodies overnight at 4°C (mouse β-actin (Sigma Aldrich

122   A3854, 1:40000); rabbit PI3K p110α (Cell signaling 4249S, 1:1000); mouse AKT (Santa

123   Cruz Biotechnology sc-5298, 1:1000); rabbit phospho-AKT (Cell signaling 4060S,

124   1:1000) and mouse CD81 (Santa Cruz Biotechnology sc-166029,1:500). As secondary

125   antibody, an HRP-conjugated goat anti-rabbit (Cell signaling 7074S, 1:3000) or anti-

126   mouse IgG antibody (Jackson Laboratory, AB_10015289,1:3000) was used. Bands were

127   visualized using a chemiluminescent substrate (Clarity Western ECL Substrate, Bio-

128   Rad) in a ChemiDoc XRS+ system (Bio-Rad) and their intensity quantified by ImageJ

129   software.

130

131   2.3.3 RNA isolation and quantitative real-time reverse-transcription PCR

132   About 24 h after transfection, cells were harvested and RNA was extracted using the

133   Trizol method following the manufacturer's instructions. RNA samples were treated with

134   DNAse I (Thermo Fisher Scientific), avoiding contamination with genomic DNA, and

135   converted to cDNA with the Xpert cDNA Synthesis Master Mix kit (Grisp). RT-PCR was

136   performed in a CFX 96 Real-Time PCR System (Bio-Rad) using the Luna Universal

137   qPCR Master Mix kit (New England Biolabs). The gene-specific primers used are

138   outlined in Table 1. Gene expression levels were normalized to the levels of the

139   housekeeping gene *18S rRNA*. Relative gene expression is presented as fold change

140   ($2-\Delta Ct$) [16] with untreated cells (control group) set to a value of 1.0.

141

142   2.3.4 Cytotoxicity evaluation

143   For cell viability assessment, cells seeded in 96 well-plates with a density of 8×10^3

144   cells per well were incubated at 37°C 5% CO_2 for 24 h prior to the transfection. After

145   completion of the transfection period, the medium was removed and cells were incubated

146   with 100 µL of MTT (0.5 mg/mL) for 2 h. Next, 100 µL of DMSO was added to solubilize

147   the intracellular MTT crystals for 10 min at RT. Cellular viability was determined by the

148   measurement of the optical density at 570 nm using a Multiskan Sky microplate reader

149   (Thermo Fisher Scientific).

150

151   2.3.5 Annexin/PI staining by flow cytometry

152   The extent of cellular apoptosis was detected 48 h post-transfection with the FITC

153   Annexin V apoptosis detection kit (BD Biosciences) according to the manufacturer's

154   recommendations. Briefly, cells (2×10^5 per condition) were harvested, rinsed with PBS

155   1×, resuspended in 1× Binding Buffer and incubated with 1 µL of AV-FITC and 1 µL PI

156   for 15 min in the dark at room temperature. The samples were analyzed using the flow

157   cytometer Epics XLTM (Beckman Coulter) counting at least 20000 events. The collected

158   data was examined with the FCS Express 6 Flow Research software.

159

160   2.3.6 Cell cycle analysis

161   The effect on cell cycle progression was determined by flow cytometry. After the

162   transfection period, adherent cells were scrapped, washed with PBS 1× and were further

163   collected by centrifugation at 2700 rpm for 3 min. Then, cells were fixed with ice-cold

164   70% ethanol for 15 min and after two centrifugations at previous conditions, the cells

165   were treated with 1 µL of ribonuclease A (RNAse A, 10 mg/mL) (Thermo Fisher

166   Scientific) and 10 µL PI (1 mg/mL), at 37°C for 30 min. Cell cycle distribution was

167 analyzed by measuring DNA content using the flow cytometer Epics XLTM (Beckman
168 Coulter), counting at least 20000 events.

169

170   2.3.7 Wound healing assay

171   In the transfection day, a straight scratch was performed with a pipette tip in the
172 cellular monolayer, after cleaning the cellular debris. Cells were maintained in DMEM,
173 without serum supplementation, observed with an optical microscope and photographed
174 at 0, 12, 24, 48 and 72 h post-transfection. The wound area was determined using the
175 ImageJ software and the scratched area percentage was obtained by area comparison
176 between the distinct time-points and the initial one.

177

178   **2.4 Exosome isolation**

179   Exosome isolation procedure was performed according to previously reported
180 protocols [17]. Briefly, culture supernatant was removed and replaced with serum-free
181 DMEM, after BJ cells achieved 80% confluency on a T175 flasks culture. After 48 h, the
182 media was collected, and cellular debris were removed by two consecutive
183 centrifugations steps at 800 × g for 5 min and 2000 × g for 10 min. The supernatant was
184 filtered with 0.2 µm Millipore Express PES Membrane Filters (Merck) and was then
185 ultracentrifuged at 100,000 × g for 3 h at 4°C. The pellet of exosomes was resuspended
186 in sterile PBS 1× and aliquoted, before storage at -80°C.

187

188   **2.5 Exosome characterization**

189   2.5.1 Size distribution and particle concentration of exosomes

190   The size distribution and particle number/concentration of exosomes were measured
191 by nanoparticle tracking analysis (NTA). Batches of BJExo were diluted in ultrapure H_2O
192 and analyzed using a Nanosight NS500 system (Malvern Instruments). For each BJExo
193 batch, two 60 sec videos were recorded, with a 25 ms camera shutter and the equipment
194 focus adjusted to achieve optimal counting. The tracking analysis tool of Nanosight NTA
195 2.3 software was utilized to analyze the results.

196

197   2.5.2 Zeta potential measurement

198   Zeta potential measurements along with size distribution of isolated exosomes were
199 performed in a Zetasizer Nano series ZS (Malvern Instruments). Samples were 10 times
200 diluted with ultrapure H_2O and transferred to appropriate capillary cuvette cells. The data
201 collected was analyzed through Zetasizer Nano software 3.3 (Malvern Panalytical).

202

203   2.5.3 Transmission electron microscopy (TEM)

204   For negative staining TEM, 10 µL of BJExo were mounted on Formvar/carbon film-
205   coated mesh nickel grids (Electron Microscopy Sciences, Hatfield, PA, USA). The liquid
206   in excess was removed with filter paper and 10 µL of 1% uranyl acetate (Sigma Aldrich)
207   were added on to the grids and left standing for 10 sec. Visualization was carried out on
208   a JEOL JEM 1400 TEM at 120 kV (Tokyo, Japan) and images were digitally recorded
209   using a CCD digital camera (Orious 1100W Tokyo, Japan) at the HEMS / i3S of the
210   University of Porto.

211

212   2.5.4 *In vitro* tracking using confocal laser scanning microscopy (CLSM)

213   BJExo were fluorescently labeled with CM-DiI. In brief, 1 µL of 1 mM DMSO stock
214   solution of CM-DiI was added to 2 or 10 µg of BJExo diluted in PBS 1×. The excess dye
215   from the labeled exosomes was removed using centrifugal filters (10 kDa, Merck). In
216   order to evaluate the BJExo intracellular localization, MDA-MB-231 cells were seeded.
217   In the next day, CM-DiI-labeled BJExo were added and incubated for 3 h. Afterwards,
218   cells were stained with DAPI and Alexa fluor 488-Phalloidin, followed by mounting on
219   slides prior to confocal laser scanning microscopy (CLSM). Images were acquired in a
220   sequential mode by a confocal scanning laser microscope (BX61 FLUOVIEW1000,
221   Olympus), using a 60× oil immersion objective and with the specific filter settings for
222   DAPI, Alexa fluor 488 and CM-DiI.

223

224   **2.6 Exosome encapsulation of siRNA via electroporation**

225   siPIK3CA was loaded into BJExo following a previously described electroporation
226   procedure [19]. Briefly, BJExo were mixed with siPIK3CA or siNC in a siRNA:BJExo ratio
227   of 1:1 or 1:2 (µg:µg) with 400 µL of electroporation buffer (1.15 mM potassium phosphate
228   pH 7.2, 25 mM potassium chloride and 21% OptiPrep). Then, the mixture was loaded
229   into pre-chilled 4 mm electroporation cuvettes (Cell projects) and electroporated using a
230   Gene Pulser Xcell Electroporation System (Eppendorf) at 400 V and 125 µF capacitance.
231   The electroporated exosomes (BJExo^siPIK3CA or BJExo^siNC) were consequently subjected
232   to ultracentrifugation at 40,000 rpm for 2 h at 4°C to remove free siRNA, the supernatant
233   was aspirated and BJExo^siPIK3CA were resuspended in DMEM.

234

235   **2.7 Statistical analysis**

236   The results from different experiments were presented as mean ± SD and analyzed

237   using GraphPad Prism 8 Software (Graphpad Holdings). The statistical significance of

238   all data was determined by two-way ANOVA using Sidak´s multiple comparisons test. P-

239   value (p) < 0.05 denoted the presence of statistically significant differences between the

240   experimental groups.

241

242   **3. Results**

243   **3.1 siPIK3CA affects PAM pathway by downregulating mRNA and protein levels**

244   This work aimed to target *PIK3CA* oncogene that, being commonly mutated in breast

245   cancer, triggers a PAM pathway hyperactivation and promotes cancer cells survival,

246   proliferation and migration (**Figure 1A**). Therefore, we examined the silencing effect of

247   *PIK3CA* in the TNBC-representative cell line MDA-MB-231 (*PIK3CA* wild-type) and in

248   the HER^{2+} MDA-MB-453 cells that harbor a *PIK3CA* and *PTEN* mutation (H1047R and

249   E307K, respectively). To perform this evaluation, RT-PCR experiments were carried out

250   24 h after cellular transfection with siPIK3CA (25 nM), assessing *PIK3CA*, *AKT* and

251   *MTOR* mRNA levels (**Figure 1B**). Indeed, siPIK3CA showed a great potential (p ≤ 0.001

252   and p ≤ 0.0001) for the inhibition of the PAM pathway in both cell lines, as suggested by

253   the expression levels of key elements of this cascade. Downregulation of *PIK3CA*, *AKT*

254   and *MTOR* levels was observed at a higher extend for the TNBC cell line: 0.25 ± 0.08,

255   0.32 ± 0.05 and 0.413 ± 0.06, respectively. Moreover, siNC transfected cells did not

256   evidence any significant reduction on mRNA expression for MDA-MB-453 cells (p > 0.05)

257   and even exhibited an increase in the expression for MDA-MB-231 cells (p ≤ 0.01)

258   (**Figure S1A**). At the protein level, the effect on the PI3K levels was evaluated through

259   western blot analysis over time. MDA-MB-231 and MDA-MB-453 cells were transfected

260   with siPIK3CA (25 nM) and the protein content was quantified 12, 24 and 48 h post-

261   transfection (**Figure 1C and 1D**) Results displayed a significant reduction (p ≤ 0.0001)

262   to 0.47 ± 0.06 (12 h) and 0.54 ± 0.09 (24 h), in MDA-MB-231 and MDA-MB-453 cells,

263   respectively. Additionally, the consequences on the signaling molecule located

264   downstream (AKT) and in its active form (phosphorylated AKT) was studied (**Figure**

265   **S1B**). Clearly, siPIK3CA has a profound impact on p-AKT expression in a dose-

266   dependent manner more pronounced for MDA-MB-231 than for MDA-MB-453 cells.

267   However, no impact on AKT total protein was achieved, independently of the siPIK3CA

268   concentration. Moreover, the protein levels of transfected cells, treated solely with

269   lipofectamine and siNC, were not affected. Since the increment of p-AKT/AKT ratio is an

270   indicator of PAM activation, the ratio was calculated for the TNBC cells and a notorious

271   decrease over time was found (**Figure S1C**). Overall, these data indicate that the

272 siPIK3CA sequence can effectively downregulate *PIK3CA* in different breast cancer cells
273 with distinct outcomes. The differences observed between both cell lines may be
274 correlated to the *PIK3CA* mutation status.

275

276 **3.2 Impairment of PAM pathway reduces breast cancer cells survival**

277 Given that the PAM pathway is enrolled in multiple cellular survival mechanisms
278 [20,21], the therapeutic effect of siPIK3CA on the viability of MDA-MB-231 and MDA-
279 MB-453 cells was studied by MTT assay (**Figure 2A** and **2B**). These cells were
280 transfected with siNC or siPIK3CA for 24, 48 or 72 h. The results indicated that the
281 *PIK3CA*-targeting siRNA (50 nM) promoted a decrease on the MDA-MB-231 and MDA-
282 MB-453 cellular viability at 48 and 72 h, while the siNC did not trigger any significant
283 reduction ($p > 0.05$). The maximum effect was detected at 48 h with a reduction to 71.6
284 ± 0.72 % and 75.7 ± 10.25 % for MDA-MB-231 and MDA-MB-453 cells, respectively. In
285 addition, siPIK3CA at 25 nM apparently only significantly affects the survival of the MDA-
286 MB-231 cell line ($p \leq 0.05$).

287

288 **3.3 *PIK3CA* knockdown increases cellular apoptosis and affects cell cycle**
289 **progression of MDA-MB-231 cells**

290 To further ascertain if the decrease in cell viability was associated with apoptosis
291 induction mediated by siPIK3CA, Annexin V/PI staining experiments were performed.
292 Given that TNBC cells were found to be more susceptible to the transfection, they were
293 selected for this experiment. The effect on cell apoptosis was evident as can be seen in
294 the flow cytometry plots with a right and upper shift of the treated samples compared to
295 the non-treated cells (**Figure 3A**). This effect was translated on an increase of necrosis
296 and early/late apoptosis mechanisms, particularly for the 50 nM condition with only 50.17
297 ± 7.09% of viable cells (**Figure 3B**). Furthermore, the percentage of apoptotic and
298 necrotic cells increased in a siPIK3CA concentration dependent manner. In addition, we
299 evaluated the effects of *PIK3CA* knockdown on cell cycle progression (**Figure 3C** and
300 **3D**). The results showed that a 50 nM concentration transfection induced a significant (p
301 ≤ 0.01) sub-G1 and S phase cellular retainment that was accompanied by an increase
302 in G0-G1, while the 25 nM concentration was insufficient to produce significant outcomes
303 (**Figure 3C** and **3D**). Therefore, the siPIK3CA-mediated transfection successfully
304 induced cellular apoptosis and cell cycle arrest.

305

306 **3.4 siPIK3CA promotes suppression of cellular migration**

307   Since metastasis is one of the major hindrances in the success of cancer therapy and

308   the PAM pathway is associated with this malignant behavior [22], the effect of siPIK3CA

309   in cancer cell migration was evaluated through an *in vitro* methodology. Based on the

310   previous results, MDA-MB-231 cells were selected to perform the migration evaluation.

311   A wound healing assay was performed. Briefly, MDA-MB-231 cells were seeded,

312   scratched, transfected and photographed over time (0, 12, 24, 48 and 72 h) (**Figure 4A**).

313   From visual inspection, while the gap from the non-treated group continuously reduces

314   in a time-dependent manner, the treated samples do not close at the same proportion.

315   This observation translates in a decreased wound healing capacity after both 25 and 50

316   nM siPIK3CA transfection since there are no statistically significant differences between

317   the two studied concentrations ($p > 0.05$) (**Figure 4B**). With a preponderant role in

318   tumorigenic metastasis, the epithelial-to-mesenchymal transition (EMT) mechanism

319   enables tumors with an increased migration and invasion capacity [23]. EMT is

320   characterized by the acquisition of mesenchymal features and loss of epithelial markers.

321   To further ascertain whether *PIK3CA* silencing affects EMT, we evaluated the expression

322   of the mesenchymal N-cadherin (*NCAD*) and the epithelial E-cadherin (*ECAD*) markers

323   (**Figure 4C**). RT-PCR evidenced a decline of *NCAD* expression to 0.29 ± 0.04 opposite

324   to the increment of *ECAD* levels to 4.41 ± 0.72. Thus, the *PIK3CA* knockdown impaired

325   the MDA-MB-231 cellular migration and promoted a reversal of the EMT mechanism.

326

327   **3.5 Isolation and characterization of BJ-derived exosomes**

328   Exosome-like nanovesicles were extracted from non-tumorigenic cells BJ (BJExo) to

329   avoid carry immunostimulatory or carcinogenic information from the parental cells [24].

330   An average size of 97.9 ± 11.26 nm and 73.13 ± 3.17 nm in diameter was retrieved by

331   NTA and dynamic light scattering, respectively (**Figure 5A, 5B and 5C**). BJExo were

332   successfully prepared and characterized within the range of accurate size (30-150 nm)

333   and with a slightly negative zeta potential of -6.38 ± 0.37 mV (**Figure 5C**). The isolated

334   BJExo were positive for the presence of the tetraspanin CD81. Moreover, the commonly

335   used exclusion marker β-actin was detected in whole cell lysates of BJ cells but not in

336   exosomes (**Figure 5D**). Then, to validate BJExo as a delivery platform, it was necessary

337   to confirm that they can be efficiently delivered to the nucleus of the intended targeted

338   cell to achieve the desired pharmacological effect. Thus, MDA-MB-231 cellular uptake

339   was tracked using CLSM (**Figure 5E**). CLSM results showed a clear internal localization

340   of BJExo using two different amounts, particularly concentrated in the nucleus,

341   confirming the successful internalization into the cells. In addition, CLSM results

342   evidenced MDA-MB-231 cellular uptake of siRNA-loaded BJExo, suggesting a

343   successful application of the electroporation protocol and siRNA delivery mediated by

344   the exosomes (**Figure S2**).

345

346   **3.6 siPIK3CA delivered by exosomes promotes a faster and greater effect**

347   Therapeutic siPIK3CA was loaded into BJExo (BJExo^{siPIK3CA}) with a 1:2 ratio

348   (siPIK3CA:BJExo; μg:μg), using electroporation. The biological activity was, firstly,

349   evaluated through RT-PCR analysis of the mRNA levels of *PIK3CA*, *AKT* and *MTOR*

350   after MDA-MB-231 (**Figure 6A**) and MDA-MB-453 (**Figure 6B**) cells treatment with

351   BJExo^{siPIK3CA} over time (3, 6 and 24 h). *PIK3CA* expression in BJExo^{siNC} and BJExo-

352   treated groups showed no statistically significant difference (p > 0.05) compared to the

353   non-treated groups (**Figure S3**), while a significant knockdown can be observed for the

354   samples treated with BJExo^{siPIK3CA}. The *PIK3CA*, *AKT* and *MTOR* mRNA levels in MDA-

355   MB-231 reduced to a maximum of 0.16 ± 0.1, 0.37 ± 0.1 and 0.31 ± 0.02; and in MDA-

356   MB-453 treated cells decreased to 0.19 ± 0.04, 0.56 ± 0.13 and 0.44 ± 0.14, respectively.

357   The cellular viability evaluation by MTT was carried out after treatment of MDA-MB-231

358   and MDA-MB-453 cells for 3, 6, 24 or 48 h with BJExo^{siPIK3CA} (**Figure 6C**). Results

359   showed that 6 h after BJExo^{siPIK3CA} treatment, MDA-MB-231 and MDA-MB-453 cellular

360   viability decreased to 52.3 ± 7.7 and 42.7 ± 1.2%, respectively. Altogether, **Figure 6A,**

361   **6B** and **6C** showed that the knockdown is more pronounced (3 and 6 h) for the shorter

362   time-points and, a cellular recovery for treatment periods over 24 h is observed, thus

363   suggesting the need for multiple dosing, due to the transient knockdown promoted by

364   the siPIK3CA. Then, we compare the maximum decrease observed on *PIK3CA* mRNA

365   levels as well as cellular viability achieved with BJExo^{siPIK3CA} in relation to the

366   lipofectamine-based transfection (Lipo^{siPIK3CA}) (**Table 2**). Clearly, BJExo^{siPIK3CA} triggered

367   a greater and faster onset, indicating BJExo as a superior carrier of siPIK3CA.

368

369   **4. Discussion**

370   The PAM signaling pathway is one of the most important and frequently active

371   intracellular cascades, assuming roles in cell proliferation, survival, cycle and

372   metabolism. Several research groups have associated the aberrant hyperactivation and

373   dysregulation of this pathway to a variety of cancers [6,7]. These alterations trigger

374   resistance to antineoplastic therapies and are promoted by several mutations, including

375   in the *PIK3CA* oncogene that represents the most common group of genomic

376   abnormalities in breast cancer [25–27]. Therefore, tremendous efforts are being

377   employed to develop anticancer strategies targeting the PAM pathway. Currently, five

378   different inhibitors targeting the PAM oncogenic signaling pathway in diverse cancers

379   have been approved by FDA [28–32]. Within the breast cancer therapy scenario,

380   alpelisib (BYL-719), a class I PIK3 α-isoform targeted inhibitor, was approved in the

381   treatment of hormone receptor positive cases with a tremendous potential in advanced

382   tumor with *PIK3CA* mutations [31,33]; and everolimus, an allosteric mTORC1 inhibitor,

383   that improved the patient outcomes after endocrine therapy in hormone and HER_2

384   positive diagnostics [28,34]. However, despite these advances there is still a lack of

385   effective targeted therapies. RNAi is a promising modality in cancer treatment, allowing

386   oncogenes expression knockdown after being successfully delivered to cells. For *in vitro*

387   experiments, lipofectamine-based transfection is considered the gold standard to

388   successfully deliver these molecules to the recipient cells.

389   In this work, we studied the downregulation of *PIK3CA* by delivering a siRNA to a

390   panel of breast cancer cell lines, including the *PIK3CA* wild-type cell line MDA-MB-231

391   and HER_{2+} cell line MDA-MB-453 that harbors the *PIK3CA* H1047R and E370K

392   oncogenic mutations. Results revealed that siPIK3CA (25 nM) led to a remarkable

393   depletion in the mRNA expression of *PIK3CA*, *AKT* and *MTOR*, more pronounced in

394   MDA-MB-231 cells than in MDA-MB-453 cell line. The same outcome was observed at

395   protein level with a notorious silencing of PI3K. The *PIK3CA* silencing promoted a

396   decrease in the protein expression of the phosphorylated AKT (phospho-AKT) in a

397   siPIK3CA dose dependent manner more noticeably in MDA-MB-231 cell line.

398   Nevertheless, no significant effect in the total AKT level was found. These outcomes are

399   in line with previous reports [35–37]. Keam et al [35] showed that head and neck cancer

400   cell lines treated with various doses of an α-isoform selective PI3K inhibitor (BYL719)

401   exhibited a reduction of phospho-AKT in a dose-dependent manner, independently of

402   *PIK3CA* mutations. The same was observed by Yuan et al [37]. These authors reported

403   that T47D (*PIK3CA* mutated) and MDA-MB-231 (no *PIK3CA* mutation) breast cell lines

404   exhibit a decrease of the phospho-AKT levels that depend on the BYL719 concentrations

405   assayed. Similar to our results, also no effects in the total AKT level were found in both

406   studies.

407   The differences observed between the results for both cell lines is probably associated

408   to the mutation profile. The *PIK3CA* mutation dysregulates and hyperactivates the PAM

409   pathway, increasing its expression and hampering its inhibition. In addition, the depletion

410   of PTEN promoted by the E370K abnormality harbored by MDA-MB-453 cells, does not

411   allow the negative control of PAM dephosphorylating PIP3 to PIP2 and, therefore,

412   contributes to the pathway activation. The present study revealed that *PIK3CA* silencing

413   was effective and induced the inhibition of AKT phosphorylation, which could suppress

414   the activity of PI3K/AKT signaling interaction.

415   Given the enrollment of PAM pathway on cell survival and proliferation, we sought to
416   study the role of siPIK3CA in the cell lines under study. The MTT assay evidenced a
417   slowdown on the cell growth particularly for the higher concentration (50 nM) and longer
418   transfection periods (48 and 72 h). However, MDA-MB-231 cells were clearly more
419   susceptible to the siPIK3CA, including a significant reduction on cellular viability with 25
420   nM, which was explained by the apoptosis and necrosis induction observed in the
421   annexin V-PI experiments. MDA-MB-231 cells were also subjected to cell cycle analysis,
422   that evidenced, 48 h post-transfection, a cellular arrest at sub-G1 and S phase
423   hampering the cellular progression to the division process. Indeed, this pro-apoptotic and
424   anti-proliferative tendency was previously reported with RNAi-based strategies targeting
425   *PIK3CA* [38–40]. Li et al [40] observed in gastric cancer cells treated with a PIK3CA-
426   targeting siRNA an increase in the same proportion of early apoptotic cells, however
427   higher effect on late apoptosis and necrosis was only achieved with a dual-targeting
428   strategy. Moreover, in their work they also observed a cellular retention at sub-G1 stage.
429   Nevertheless, Zhang and collaborators [41] showed that different dosages of a potent
430   PI3K inhibitor promoted a more expressive cell growth inhibition in breast cancer cells
431   harboring *PIK3CA* mutations than wild-type cell lines, which is not supported by the
432   collected data. This difference can be associated to the distinct pharmacological
433   inhibition employed.

434   To further validate *PIK3CA* downregulation impact, migration studies were conducted
435   with MDA-MB-231 cells. The wound healing assay indicated that the transfection
436   promoted an impairment on cellular recovery and migratory capacity for at least 72 h with
437   either 25 or 50 nM concentrations. This impact in cellular migration upon treatment with
438   siPIK3CA could be explained in part by the reversal of the EMT mechanism as verified
439   by the downregulation of N-cadherin and upregulation of E-cadherin expression levels.
440   Similar outcomes have already been reported [38,42,43]. For example, Guerreiro and
441   co-workers [38] concluded that medulloblastoma cells DAOY transfected with a *PIK3CA*-
442   targeting siRNA displayed a decreased migration capacity of 30 to 40%. Deng et al [42]
443   showed that ovarian cancer cells treated with a dual PI3K/mTOR inhibitor (BEZ235)
444   exhibited an EMT reversal phenomenon, as observed in this work.

445   Although RNAi has revolutionized the gene silencing field, there are some underling
446   hindrances to overcome, such as the difficulties to safely deliver these molecules.
447   Exosomes that are nanosized natural vesicles emerged as possible siRNA carriers [15].
448   Herein, we report the efficient loading of siRNA molecules into BJ derived exosomes by
449   performing electroporation. Exosome-like nanovesicles were isolated in this study with
450   an average size of 97.9 nm and a slightly negative zeta potential of -6.38 mV. Moreover,
451   they were positive for the presence of the common exosome marker CD81 and negative

452   for the exclusion marker β-actin. This BJ-derived exosomes characterization is in

453   agreement with other well-documented reports [17,44].

454   After exosome loading with siPIK3CA, a clear faster and improved reduction of

455   *PIK3CA*, *AKT* and *MTOR* mRNA levels was observed for MDA-MB-231 and MDA-MB-

456   453 cells in relation to the onset obtained with lipofectamine transfection. Additionally,

457   exosome-based delivery of siPIK3CA promoted a rapid decrease of cell viability between

458   50-56% in both cell lines, being observed a cellular recovery for treatment times superior

459   to 24 h. Interestingly, the use of a different carrier, exosomes instead lipofectamine,

460   seemed to annul the previously observed differences in *PIK3CA* silencing and cell

461   survival between the two cell lines. In other words, with the use of exosomes as delivery

462   vehicles, the *PIK3CA* status does not appear to influence the outcome and this strategy

463   produces favorable results independently of the mutations profile. Overall, our results

464   showed that siPIK3CA carried by exosomes achieved a more rapid and earlier onset on

465   gene expression silencing and cellular viability, compared with lipofectamine-based

466   transfection. Although some differences between cell lines were found, the main effects

467   are promoted within the 6 h range and a cellular recovery is observed after the timepoint

468   corresponding to 24 h.

469   Previous reports have already studied the potential acute cytotoxicity of fibroblast-

470   derived exosomes. For example, Kamerkar et al [45], that also described the isolation of

471   BJ-derived exosomes through differential centrifugation processes, showed that

472   exosomes without siRNA did not induce any decrease on cellular viability of pancreatic

473   cancer cells. Yet, unspecific effects on non-tumorigenic cell lines, as well as on other

474   breast cancer cell lines could be evaluated in the future, to ascertain if similar outcomes

475   are obtained. Nevertheless, it is important to note that other authors have shown, both

476   suing *in vitro* and *in vivo* studies, that siRNA loaded into exosomes is a safe delivery

477   strategy [45,46].

478   Although the electroporation efficiency was not determined, the amount of siPIK3CA

479   loaded into the BJExo was less than the 25 nM concentration used with the

480   lipofectamine-based approach. In fact, independently of the loading success, with less

481   siRNA the effect observed with the exosomes was more significant. Similar

482   achievements were observed by Xu et al [46]. Those authors observed that the delivery

483   of PAK4-RNAi by PANC-derived exosomes promoted an improved and faster inhibitory

484   outcome on pancreatic cancer cells *in vitro* comparing with the lipofectamine approach.

485   In addition, tumor volume growth reduction and survival decline were observed *in vivo*

486   after a group of dosages, suggesting the need of multiple dosing. Despite the different

487   targeted oncogene and type of cancer, as well as a distinct EVs source, the more efficient

488   outcomes obtained in both works are probably associated to the use of exosomes as

489 delivery vehicles. While lipofectamine relies on the complex formation between the
490 cationic lipid with the negatively charged siRNA backbone which can expose the siRNA
491 to degradation, exosomes confine the siRNA within the double layer membrane, thus
492 offering better siRNA protection during delivery [47]. Moreover, Murphy et al [48] claim
493 that EVs deliver siRNA several orders of magnitude more efficiently than synthetic
494 systems. Both reports are well-aligned with our study [46,48].

495   Exosomes fuse with the plasma membrane and release their contents into the cytosol.
496 Exosome cargoes, as siRNA, can undertake multiple routes to bypass direct lysosomal
497 degradation to fulfill their signaling functions. Several studies, including ours,
498 demonstrate exosome-mediated functional changes in recipient cells [45,46]. To achieve
499 increased duration effects on viability, multidose administrations of BJExo^{siPIK3CA}, instead
500 of a single dose administration as we did in our study, should be considered in the future.
501 The rationale of exosome dose selection, as well as the treatment frequency are
502 extremely important parameters to be considered mainly in *in vivo* experiments.
503 Moreover, the underlying interaction mechanisms between exosomes and siRNA needs
504 further evaluation to pave the way to the development of novel therapies.

505

506 **5. Conclusions**

507   The present study concluded that *PIK3CA* silencing mediated by a siRNA-targeting
508 approach (siPIK3CA) ameliorates breast cancer outcomes. The impairment of the PAM
509 pathway, by disrupting gene and protein expression, promoted an apoptotic and anti-
510 proliferative effect. In addition, the cell migration capacity was reduced upon treatment
511 with siPIK3CA, hindering the metastasis process. However, using lipofectamine as the
512 delivery agent, the *PIK3CA* mutation status hampered siPIK3CA action. The use of an
513 effective and safe delivery method was also explored by loading siPIK3CA onto BJ-
514 derived exosomes. A greater and faster effect in relation to the lipofection approach was
515 observed. In conclusion, this study validates the PAM pathway and, in particular, *PIK3CA*
516 as a target for breast cancer therapy and introduces BJ-derived exosomes as a superior
517 carrier that increments the observed impairment.

518

519   **Author Contributions:** LR conceived and supervised the study. RS and DF
520 performed the experiments, analyzed the data and wrote the manuscript. LR and DF
521 gave suggestions on the experimental design. All authors reviewed the results and
522 approved the final version of the manuscript.

523

532

533   **Conflicts of Interest:** The authors declare no conflict of interest.

534

535   **References**

536   [1]   H. Sung, J. Ferlay, R.L. Siegel, M. Laversanne, I. Soerjomataram, A. Jemal, F.
537   Bray, Global Cancer Statistics 2020: GLOBOCAN Estimates of Incidence and
538   Mortality Worldwide for 36 Cancers in 185 Countries, CA. Cancer J. Clin. 71
539   (2021) 209–249. https://doi.org/10.3322/caac.21660.

540   [2]   G. Bianchini, C. De Angelis, L. Licata, L. Gianni, Treatment landscape of triple-
541   negative breast cancer — expanded options, evolving needs, Nat. Rev. Clin.
542   Oncol. 2021. (2021) 1–23. https://doi.org/10.1038/s41571-021-00565-2.

543   [3]   V.B. Wali, G.A. Patwardhan, V. Pelekanou, T. Karn, J. Cao, A. Ocana, Q. Yan,
544   B. Nelson, C. Hatzis, L. Pusztai, Identification and Validation of a Novel Biologics
545   Target in Triple Negative Breast Cancer, Sci. Rep. 9 (2019) 1–10.
546   https://doi.org/10.1038/s41598-019-51453-w.

547   [4]   T.F.S. Mendes, L.D. Kluskens, L.R. Rodrigues, Triple Negative Breast Cancer:
548   Nanosolutions for a Big Challenge, Adv. Sci. 2 (2015) 1500053.
549   https://doi.org/10.1002/advs.201500053.

550   [5]   M.A. Khan, V.K. Jain, M. Rizwanullah, J. Ahmad, K. Jain, PI3K/AKT/mTOR
551   pathway inhibitors in triple-negative breast cancer: a review on drug discovery
552   and future challenges, Drug Discov. Today. 24 (2019) 2181–2191.
553   https://doi.org/10.1016/j.drudis.2019.09.001.

554   [6]   F. Janku, T.A. Yap, F. Meric-Bernstam, Targeting the PI3K pathway in cancer:
555   Are we making headway?, Nat. Rev. Clin. Oncol. 15 (2018) 273–291.
556   https://doi.org/10.1038/nrclinonc.2018.28.

557   [7]   L. Yu, J. Wei, P. Liu, Attacking the PI3K/Akt/mTOR signaling pathway for
558   targeted therapeutic treatment in human cancer, Semin. Cancer Biol. (2021).

559   https://doi.org/10.1016/j.semcancer.2021.06.019.

560   [8]   J. Pascual, N.C. Turner, Targeting the PI3-kinase pathway in triple-negative

561   breast cancer, Ann. Oncol. 30 (2019) 1051–1060.

562   https://doi.org/10.1093/annonc/mdz133.

563   [9]   G. Shan, RNA interference as a gene knockdown technique, Int. J. Biochem.

564   Cell Biol. 42 (2010) 1243–1251. https://doi.org/10.1016/j.biocel.2009.04.023.

565   [10]   B. Hu, L. Zhong, Y. Weng, L. Peng, Y. Huang, Y. Zhao, X.-J. Liang, Therapeutic

566   siRNA: state of the art, Signal Transduct. Target. Ther. 5 (2020) 101.

567   https://doi.org/10.1038/s41392-020-0207-x.

568   [11]   H. Dana, G.M. Chalbatani, H. Mahmoodzadeh, R. Karimloo, O. Rezaiean, A.

569   Moradzadeh, N. Mehmandoost, F. Moazzen, A. Mazraeh, V. Marmari, M.

570   Ebrahimi, M.M. Rashno, S.J. Abadi, E. Gharagouzlo, Molecular Mechanisms

571   and Biological Functions of siRNA., Int. J. Biomed. Sci. 13 (2017) 48–57.

572   http://www.ncbi.nlm.nih.gov/pubmed/28824341.

573   [12]   M.M. Zhang, R. Bahal, T.P. Rasmussen, J.E. Manautou, X. bo Zhong, The

574   growth of siRNA-based therapeutics: Updated clinical studies, Biochem.

575   Pharmacol. 189 (2021). https://doi.org/10.1016/j.bcp.2021.114432.

576   [13]   L. Doyle, M. Wang, Overview of Extracellular Vesicles, Their Origin,

577   Composition, Purpose, and Methods for Exosome Isolation and Analysis, Cells.

578   8 (2019) 727. https://doi.org/10.3390/cells8070727.

579   [14]   S.M. Patil, S.S. Sawant, N.K. Kunda, Exosomes as drug delivery systems: A

580   brief overview and progress update, Eur. J. Pharm. Biopharm. 154 (2020) 259–

581   269. https://doi.org/10.1016/J.EJPB.2020.07.026.

582   [15]   D. Ferreira, J.N. Moreira, L.R. Rodrigues, New Advances in Exosome-based

583   Targeted Drug Delivery Systems, Crit. Rev. Oncol. Hematol. (2022) 103628.

584   https://doi.org/10.1016/j.critrevonc.2022.103628.

585   [16]   M. Zhang, X. Zang, M. Wang, Z. Li, M. Qiao, H. Hu, D. Chen, Exosome-based

586   nanocarriers as bio-inspired and versatile vehicles for drug delivery: recent

587   advances and challenges, J. Mater. Chem. B. 7 (2019) 2421–2433.

588   https://doi.org/10.1039/C9TB00170K.

589   [17]   S. Kamerkar, V.S. LeBleu, H. Sugimoto, S. Yang, C.F. Ruivo, S.A. Melo, J.J.

590   Lee, R. Kalluri, Exosomes facilitate therapeutic targeting of oncogenic KRAS in

591   pancreatic cancer, Nature. 546 (2017) 498–503.

592   https://doi.org/10.1038/nature22341.

593   [18]   Y. Zhou, Y. Yuan, M. Liu, X. Hu, Y. Quan, X. Chen, Tumor-specific delivery of

594   KRAS siRNA with iRGD-exosomes efficiently inhibits tumor growth, ExRNA. 1

595   (2019) 28. https://doi.org/10.1186/s41544-019-0034-9.

596 [19] S. El-Andaloussi, Y. Lee, S. Lakhal-Littleton, J. Li, Y. Seow, C. Gardiner, L.

597   Alvarez-Erviti, I.L. Sargent, M.J.A. Wood, Exosome-mediated delivery of siRNA

598   in vitro and in vivo., Nat. Protoc. 7 (2012) 2112–26.

599   https://doi.org/10.1038/nprot.2012.131.

600 [20] S.H. Shahcheraghi, V. Tchokonte-Nana, M. Lotfi, M. Lotfi, A. Ghorbani, H.R.

601   Sadeghnia, Wnt/beta-catenin and PI3K/Akt/mTOR Signaling Pathways in

602   Glioblastoma: Two Main Targets for Drug Design: A Review, Curr. Pharm. Des.

603   26 (2020) 1729–1741. https://doi.org/10.2174/1381612826666200131100630.

604 [21] J. Shi, D. Yao, W. Liu, N. Wang, H. Lv, G. Zhang, M. Ji, L. Xu, N. He, B. Shi, P.

605   Hou, Highly frequent PIK3CA amplification is associated with poor prognosis in

606   gastric cancer, BMC Cancer. 12 (2012) 1–11. https://doi.org/10.1186/1471-2407-

607   12-50/TABLES/3.

608 [22] J.F. Liu, X.K. Zhou, J.H. Chen, G. Yi, H.G. Chen, M.C. Ba, S.Q. Lin, Y.C. Qi, Up-

609   regulation of PIK3CA promotes metastasis in gastric carcinoma, World J.

610   Gastroenterol. 16 (2010) 4986–4991. https://doi.org/10.3748/wjg.v16.i39.4986.

611 [23] C.Y. Loh, J.Y. Chai, T.F. Tang, W.F. Wong, G. Sethi, M.K. Shanmugam, P.P.

612   Chong, C.Y. Looi, The E-Cadherin and N-Cadherin Switch in Epithelial-to-

613   Mesenchymal Transition: Signaling, Therapeutic Implications, and Challenges,

614   Cells 2019, Vol. 8, Page 1118. 8 (2019) 1118.

615   https://doi.org/10.3390/CELLS8101118.

616 [24] P. Kucharzewska, H.C. Christianson, J.E. Welch, K.J. Svensson, E. Fredlund,

617   M. Ringnér, M. Mörgelin, E. Bourseau-Guilmain, J. Bengzon, M. Belting,

618   Exosomes reflect the hypoxic status of glioma cells and mediate hypoxia-

619   dependent activation of vascular cells during tumor development, Proc. Natl.

620   Acad. Sci. U. S. A. 110 (2013) 7312–7317.

621   https://doi.org/10.1073/pnas.1220998110.

622 [25] F. Rascio, F. Spadaccino, M.T. Rocchetti, G. Castellano, G. Stallone, G.S. Netti,

623   E. Ranieri, The pathogenic role of PI3K/AKT pathway in cancer onset and drug

624   resistance: an updated review, Cancers (Basel). 13 (2021).

625   https://doi.org/10.3390/cancers13163949.

626 [26] A. Ocana, F. Vera-Badillo, M. Al-Mubarak, A.J. Templeton, V. Corrales-Sanchez,

627   L. Diez-Gonzalez, M.D. Cuenca-Lopez, B. Seruga, A. Pandiella, E. Amir,

628   Activation of the PI3K/mTOR/AKT Pathway and Survival in Solid Tumors:

629   Systematic Review and Meta-Analysis, PLoS One. 9 (2014) e95219.

630   https://doi.org/10.1371/JOURNAL.PONE.0095219.

631 [27] W. Xiao, G. Zhang, B. Chen, X. Chen, L. Wen, J. Lai, X. Li, M. Li, H. Liu, J. Liu,

632   H. Han-Zhang, A. Lizaso, N. Liao, Mutational Landscape of PI3K-AKT-mTOR

633   Pathway in Breast Cancer: Implications for Targeted Therapeutics, J. Cancer. 12

634   (2021) 4408. https://doi.org/10.7150/JCA.52993.

635 [28] J. Hasskarl, Everolimus, in: Recent Results Cancer Res., Springer, Cham, 2018:

636   pp. 101–123. https://doi.org/10.1007/978-3-319-91442-8_8.

637 [29] G. Hudes, M. Carducci, P. Tomczak, J. Dutcher, R. Figlin, A. Kapoor, E.

638   Staroslawska, J. Sosman, D. McDermott, I. Bodrogi, Z. Kovacevic, V. Lesovoy,

639   I.G.H. Schmidt-Wolf, O. Barbarash, E. Gokmen, T. O'Toole, S. Lustgarten, L.

640   Moore, R.J. Motzer, Temsirolimus, Interferon Alfa, or Both for Advanced Renal-

641   Cell Carcinoma, N. Engl. J. Med. 356 (2007) 2271–2281.

642   https://doi.org/10.1056/NEJMoa066838.

643 [30] A. Kumar, R. Bhatia, P. Chawla, D. Anghore, V. Saini, R.K. Rawal, Copanlisib:

644   Novel PI3K Inhibitor for the Treatment of Lymphoma, Anticancer. Agents Med.

645   Chem. 20 (2020) 1158–1172.

646   https://doi.org/10.2174/1871520620666200317105207.

647 [31] A. Markham, Alpelisib: First Global Approval, Drugs. 79 (2019) 1249–1253.

648   https://doi.org/10.1007/s40265-019-01161-6.

649 [32] V. Pandey, A. Tripathi, A. Rani, P.K. Dubey, Deoxyelephantopin, a novel

650   naturally occurring phytochemical impairs growth, induces G2/M arrest, ROS-

651   mediated apoptosis and modulates lncRNA expression against uterine

652   leiomyoma, Biomed. Pharmacother. 131 (2020) 110751.

653   https://doi.org/10.1016/J.BIOPHA.2020.110751.

654 [33] R.R.Y. Bheemanaboina, Isoform-Selective PI3K Inhibitors for Various Diseases,

655   Curr. Top. Med. Chem. 20 (2020) 1074–1092.

656   https://doi.org/10.2174/1568026620666200106141717.

657 [34] M.E. Royce, D. Osman, Everolimus in the Treatment of Metastatic Breast

658   Cancer, Breast Cancer Basic Clin. Res. 9 (2015) BCBCR.S29268.

659   https://doi.org/10.4137/BCBCR.S29268.

660 [35] B. Keam, S. Kim, Y.-O. Ahn, T.M. Kim, S.-H. Lee, D.-W. Kim, D.S. Heo, In vitro

661   anticancer activity of PI3K alpha selective inhibitor BYL719 in head and neck

662   cancer., Anticancer Res. 35 (2015) 175–82.

663   https://ar.iiarjournals.org/content/35/1/175/tab-article-info (accessed July 5,

664   2021).

665 [36] M.J. Kim, S.J. Lee, J.H. Ryu, S.H. Kim, I.C. Kwon, T.M. Roberts, Combination of
666   KRAS gene silencing and PI3K inhibition for ovarian cancer treatment, J.
667   Control. Release. 318 (2020) 98–108.
668   https://doi.org/10.1016/J.JCONREL.2019.12.019.

669 [37] Y. Yuan, W. Wen, S.E. Yost, Q. Xing, J. Yan, E.S. Han, J. Mortimer, J.H. Yim,
670   Combination therapy with BYL719 and LEE011 is synergistic and causes a
671   greater suppression of p-S6 in triple negative breast cancer., Sci. Rep. 9 (2019)
672   7509–7509. https://doi.org/10.1038/S41598-019-43429-7.

673 [38] A.S. Guerreiro, S. Fattet, B. Fischer, T. Shalaby, S.P. Jackson, S.M.
674   Schoenwaelder, M.A. Grotzer, O. Delattre, A. Arcaro, Targeting the PI3K p110α
675   Isoform Inhibits Medulloblastoma Proliferation, Chemoresistance, and Migration,
676   Clin. Cancer Res. 14 (2008) 6761–6769. https://doi.org/10.1158/1078-
677   0432.CCR-08-0385.

678 [39] S. Reagan-Shaw, N. Ahmad, RNA Interference–Mediated Depletion of
679   Phosphoinositide 3-Kinase Activates Forkhead Box Class O Transcription
680   Factors and Induces Cell Cycle Arrest and Apoptosis in Breast Carcinoma Cells,
681   Cancer Res. 66 (2006) 1062–1069. https://doi.org/10.1158/0008-5472.CAN-05-
682   1018.

683 [40] R. Li, W.-C. Chen, X.-Q. Pang, W.-Y. Tian, W.-P. Wang, X.G. Zhang, Effect of
684   PI3K gene silencing on growth, migration and related proteins expression of
685   CD40 signal-mediated gastric cancer cells., Mol. Biol. Rep. 40 (2013) 999–1008.
686   https://doi.org/10.1007/s11033-012-2141-7.

687 [41] H. Zhang, G. Liu, M. Dziubinski, Z. Yang, S.P. Ethier, G. Wu, Comprehensive
688   analysis of oncogenic effects of PIK3CA mutations in human mammary epithelial
689   cells, Breast Cancer Res. Treat. 112 (2008) 217–227.
690   https://doi.org/10.1007/s10549-007-9847-6.

691 [42] J. Deng, X. Bai, X. Feng, J. Ni, J. Beretov, P. Graham, Y. Li, Inhibition of
692   PI3K/Akt/mTOR signaling pathway alleviates ovarian cancer chemoresistance
693   through reversing epithelial-mesenchymal transition and decreasing cancer stem
694   cell marker expression., BMC Cancer. 19 (2019) 618.
695   https://doi.org/10.1186/s12885-019-5824-9.

696 [43] S. Lee, E.J. Choi, E.J. Cho, Y. Bin Lee, J.H. Lee, S.J. Yu, J.H. Yoon, Y.J. Kim,
697   Inhibition of PI3K/Akt signaling suppresses epithelial-to-mesenchymal transition
698   in hepatocellular carcinoma through the Snail/GSK-3/beta-catenin pathway, Clin.

699   Mol. Hepatol. 26 (2020) 529–539. https://doi.org/10.3350/CMH.2019.0056N.

700   [44]   M. Mendt, S. Kamerkar, H. Sugimoto, K.M. McAndrews, C.-C. Wu, M. Gagea, S.

701   Yang, E.V.R. Blanko, Q. Peng, X. Ma, J.R. Marszalek, A. Maitra, C. Yee, K.

702   Rezvani, E. Shpall, V.S. LeBleu, R. Kalluri, Generation and testing of clinical-

703   grade exosomes for pancreatic cancer, JCI Insight. 3 (2018).

704   https://doi.org/10.1172/jci.insight.99263.

705   [45]   S. Kamerkar, V.S. LeBleu, H. Sugimoto, S. Yang, C.F. Ruivo, S.A. Melo, J.J.

706   Lee, R. Kalluri, Exosomes facilitate therapeutic targeting of oncogenic KRAS in

707   pancreatic cancer, Nature. 546 (2017) 498–503.

708   https://doi.org/10.1038/nature22341.

709   [46]   L. Xu, F.N. Faruqu, Y.M. Lim, K.Y. Lim, R. Liam-Or, A.A. Walters, P. Lavender,

710   D. Fear, C.M. Wells, J. Tzu-Wen Wang, K.T. Al-Jamal, Exosome-mediated RNAi

711   of PAK4 prolongs survival of pancreatic cancer mouse model after loco-regional

712   treatment, Biomaterials. 264 (2021) 120369.

713   https://doi.org/10.1016/j.biomaterials.2020.120369.

714   [47]   F. Pi, D.W. Binzel, T.J. Lee, Z. Li, M. Sun, P. Rychahou, H. Li, F. Haque, S.

715   Wang, C.M. Croce, B. Guo, B.M. Evers, P. Guo, Nanoparticle orientation to

716   control RNA loading and ligand display on extracellular vesicles for cancer

717   regression, Nat. Nanotechnol. 2017 131. 13 (2017) 82–89.

718   https://doi.org/10.1038/s41565-017-0012-z.

719   [48]   D.E. Murphy, O.G. de Jong, M.J.W. Evers, M. Nurazizah, R.M. Schiffelers, P.

720   Vader, Natural or synthetic RNA delivery: A stoichiometric comparison of

721   extracellular vesicles and synthetic nanoparticles, Nano Lett. 21 (2021) 1888–

722   1895. https://doi.org/10.1021/acs.nanolett.1c00094.

723

724

725

726

727   **Tables**

Gene	Primer sequences	
	Forward (5'-3')	Reverse (5'-3')
PIK3CA	GAGACATCAGCATGGCTCAA	TGTCCCTACCAACCAGAAGG
AKT	CGTCCACCAAGAAGCTGAG	GCCGTCAGAAAACATGTCAG
MTOR	AGCCTGGGTCAAAGAAGTCA	GCCAACCCTCCTTCACAATA

NCAD	GACTTGCGAAACTCCAGACC	CCATTAAGCCGAGTGATGGT
ECAD	AGATCCTGAGCTCCCTGACA	ACAGCTGTTGCTGTTGTGCT
18S	AAACGGCTACCACATCCAAG	CCTCCAATGGATCCTCGTTA

18S: 18S rRNA; *AKT*: protein kinase B; *ECAD*: E-cadherin; *MTOR*: mammalian target of rapamycin; *NCAD*: N-cadherin; *PIK3CA*: phosphoinositide 3-kinase

Table 2: Comparison of the maximum onset promoted by Lipo[siPIK3CA] with BJExo[siPIK3CA] on the *PIK3CA* mRNA expression and cellular viability

Cells	Strategy	Effect on *PIK3CA* mRNA expression [a]		Effect on cell viability (MTT) [b]	
		Maximum (fold change) [c]	Time (hours)	Maximum (%) [c]	Time (hours)
MDA-MB-231	Lipo[siPIK3CA]	0.25±0.08	24	71.6±0.7	48
	BJExo[siPIK3CA]	0.16±0.10	6	52.3±7.7	6
MDA-MB-453	Lipo[siPIK3CA]	0.66±0.10	24	77.1±4.2	72
	BJExo[siPIK3CA]	0.19±0.04	3	42.7±1.2	6

728 **Table 1:** RT-PCR primer sequences

729 [a] mRNA expression assessed by RT-PCR.
730 [b] Cellular viability obtained through MTT assay.
731 [c] Results are expressed as mean ± SD of three independent experiments.
732

733 **Captions**

734 **Figure 1: Evaluation of siPIK3CA effect on PAM pathway through western blot and RT-**
735 **PCR. (A)** Simplified illustration of the PI3K/AKT/mTOR pathway. The AKT signaling cascade is
736 activated by RTK and other stimuli that recruit PI3K, which catalyzes the conversion of
737 membrane-bound PIP2-PIP3. Next, AKT and PDK1 are activated through binding to PIP3. PTEN
738 inhibits AKT by dephosphorylating PIP3. AKT regulates cell growth through its effects on the
739 TSC1/2 complex and mTORC signaling. When the complex is activated, the downstream Rheb-
740 GTP is converted to Rheb-GDP, which stabilizes mTORC1. mTORC1 triggers cell growth and
741 proliferation by phosphorylating p70 S6 and 4E-BP1. phosphatidylinositol 3-kinase (PI3K); protein
742 kinase B (AKT); receptor tyrosine kinase (RTK); 3-phosphoinositol-dependent protein kinase-1
743 (PDK1); phosphatase and tensin homolog (PTEN); phosphatidylinositol 4,5-bisphosphate (PIP2);
744 phosphatidylinositol (3,4,5) trisphosphate (PIP3); Ras homolog enriched in brain (Rheb);
745 mechanistic target of rapamycin complex (mTORC); tuberous sclerosis proteins 1 and 2
746 (TSC1/2); ribosomal protein S6 kinase beta-1 (p70 S6K); eukaryotic translation initiation factor
747 4E (eIF4E)-binding protein 1 (4E-BP1); rapamycin-insensitive companion of mammalian target of
748 rapamycin (RICTOR); regulatory associated protein of mTOR (RAPTOR); DEP domain
749 containing mTOR interacting protein (DEPTOR); Ras homolog enriched in brain (Rheb);
750 mammalian lethal with secretory 13 protein 8 (GβL). Created with BioRender.com. **(B)** Relative
751 quantification of *PIK3CA*, *AKT* and *MTOR* mRNA levels in MDA-MB-231 and MDA-MB-453 cells
752 treated with siPIK3CA (25 nM) for 24 h. **(C)** PI3K expression level in MDA-MB-231 and MDA-MB-
753 453 non-treated cells or treated with siPIK3CA (25 nM) for 12, 24 and 48 h. **(D)** Relative
754 densiometric analysis of the expression of PI3K protein normalized to the loading control β-actin
755 and to the untreated cells, where the expression equal to 1 is represented by the dashed red line.
756 All data from (B) and (D) is expressed as the mean ± SD of three independent experiments. Two-
757 way ANOVA indicates statistically significant differences within the group assessed by Sidak's
758 post-test and denoted as follows: ns $p > 0.05$, *$p ≤ 0.05$, **$p ≤ 0.01$, ***$p ≤ 0.001$ and ****$p ≤$
759 0.0001.

760 **Figure 1: Assessment of the cellular viability impairment promoted by siPIK3CA.** Evaluation
761 of **(A)** MDA-MB-231 and **(B)** MDA-MB-453 cellular viability treated with siNC or siPIK3CA (25 or
762 50 nM) over time (24, 48 and 72 h). For each time point, viability was estimated by the 3-(4,5-
763 Dimethylthiazol-2-yl)-2,5-Diphenyltetrazolium Bromide (MTT) assay, normalized to untreated
764 cells. All data is presented as the percentage of cell viability ± SD of three independent
765 experiments. Two-way ANOVA indicates statistically significant differences within the group
766 assessed by Sidak's post-test and denoted as follows: ns $p > 0.05$, *$p ≤ 0.05$ and **$p ≤ 0.01$.

767 **Figure 2: Evaluation of the siPIK3CA effect on cellular cycle and apoptosis. (A)** Apoptosis
768 determined by Annexin V fluorescein isothiocyanate (AV-FITC) and propidium iodide (PI) assay
769 in MDA-MB-231 cells treated with siPIK3CA (25 nM or 50 nM) for 48 h. Representative histograms
770 of cells double-stained with AV and PI along with the corresponding **(B)** quantitative analysis. **(C)**
771 Cell cycle determined by PI assay in MDA-MB-231 cells treated with siPIK3CA (25 or 50 nM) for

772   48 h. Flow cytometry representative progression plots of cells stained with PI along with the

773   corresponding **(D)** quantitative analysis. Data from (B) and (D) is presented as the percentage of

774   cells ± SD of three independent experiments. Two-way ANOVA indicates statistically significant

775   differences within the group assessed by Sidak's post-test and denoted as follows: ns $p > 0.05$,

776   *$p \leq 0.05$, **$p \leq 0.01$, ***$p \leq 0.001$ and ****$p \leq 0.0001$.

777   **Figure 3: Effect of siPIK3CA on cell migration. (A)** MDA-MB-231 cells were seeded,

778   transfected with siPIK3CA (25 or 50 nM), scratched and imaged over time (0, 12, 24, 48 and 72

779   h). Scale bar: 100 µm. **(B)** The scratched area (between two white lines) was determined using

780   ImageJ and the wound closure percentage calculated **(C)** Relative quantification of *ECAD* and

781   *NCAD* mRNA levels in MDA-MB-231 cells treated with siPIK3CA (25 nM) for 24 h. Data shown in

782   (B) and (C) is presented as the wound closure percentage/fold change ± SD of three independent

783   experiments. Two-way ANOVA indicates statistically significant differences within the group

784   assessed by Sidak's post-test and denoted as follows: ns $p > 0.05$, *$p \leq 0.05$ **$p \leq 0.01$ and ***p
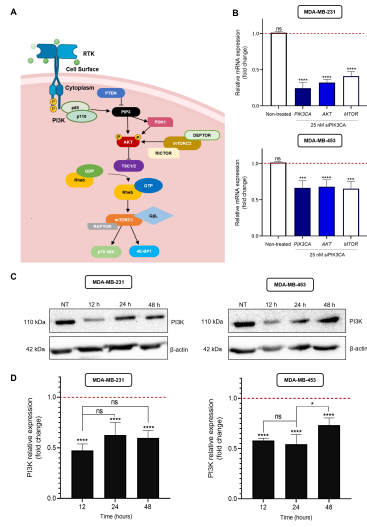
785   ≤ 0.001.

786   **Figure 5: Isolation and characterization of exosomes derived from the fibroblastic cells BJ.**

787   **(A)** Size distribution (nm) and concentration (exosomes/mL) characterization using nanoparticle

788   tracking analysis. **(B)** Negative-staining transmission electron microscopy of purified BJExo.

789   Scale bar, 200 nm. **(C)** Size and zeta potential of the BJExo retrieved by ultracentrifugation. Data

790   is presented as the mean ± SD of three independent experiments. **(D)** Representative Western

791   blot for exosome marker CD81 and exclusion marker β-actin. Cell, BJ cell lysate; BJExo, BJ

792   exosomes **(E)** Assessment of MDA-MB-231 cellular internalization of two amounts of CM-DiI-

793   labelled exosomes, 2 or 10 µg, 3 h after administration by confocal laser scanning microscopy

794   images. BJExo are labelled with CM-DiI (red), nuclei stained with DAPI (blue) and actins with

795   Alexa fluor-488 phalloidin (green). Scale bar: 40 µm.

796   **Figure 6: Inhibitory effect of siPIK3CA encapsulated in BJExo.** Relative quantification of

797   *PIK3CA*, *AKT* and *MTOR* mRNA levels in **(A)** MDA-MB-231 and (**B**) MDA-MB-453 cells treated

798   with exosomes loaded with siPIK3CA (BJExo^siPIK3CA) over time (3, 6 and 24 h). All data is

799   expressed as the fold change ± SD of three independent experiments to control after

800   normalization to the reference gene (18S rRNA). Two-way ANOVA indicates statistically

801   significant differences within the group assessed by Sidak's post-test and denoted as follows: ns

802    $p > 0.05$, *$p \leq 0.05$, **$p \leq 0.01$, ***$p \leq 0.001$ and ****$p \leq 0.0001$. **(C)** Assessment of MDA-MB-231

803   and MDA-MB-453 cellular viability treated with BJExo^siPIK3CA over time (3, 6, 24 and 48 h). For

804   each time point, viability was estimated by the 3-(4,5-Dimethylthiazol-2-yl)-2,5-

805   Diphenyltetrazolium Bromide (MTT) assay, normalized to untreated cells. Data is expressed as

806   the percentage ± SD of three independent experiments. Two-way ANOVA indicates statistically

807   significant differences within the group assessed by Sidak's post-test and denoted as follows: ns

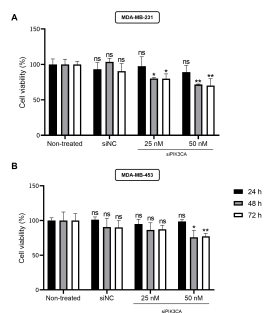808 $p > 0.05$, **$p \leq 0.01$, ***$p \leq 0.001$ and ****$p \leq 0.0001$.

809 **Figure S1: Evaluation of siPIK3CA inhibitory effect (A)** Relative quantification of *PIK3CA*
810 mRNA levels in MDA-MB-231 and MDA-MB-453 non-treated cells or treated with a negative
811 control siRNA (siNC) (25 nM) for 24 h. **(B)** Representative images of western blot analysis of the
812 protein expression level of AKT and phospho-AKT in MDA-MB-231 and MDA-MB-453 cells
813 treated with only lipofectamine (Mock), with a negative control siRNA (siNC) (25 nM) and with
814 siPIK3CA (10 nM, 25 nM, 50 nM, 75 nM or 100 nM) for 48 h. **(C)** Assessment of p-Akt/Akt protein
815 expression over time (12, 24, 48 and 72 h) after siPIK3CA (25 nM) transfection onto MDA-MB-
816 231 cells. All data in (A) and (C) is presented as the fold-change $\pm$ SD of three independent
817 experiments with similar outcomes relative to the untreated condition after normalization to the
818 reference gene (18S rRNA). Two-way ANOVA indicates statistically significant differences within
819 the group assessed by Sidak's post-test and denoted as follows: ns $p > 0.05$, *$p \leq 0.05$, **$p \leq$
820 0.01, ***$p \leq 0.001$ and ****$p \leq 0.0001$.

821 **Figure S2: Cellular internalization of TYE 563-labelled siRNA loaded into BJExo**. Confocal
822 laser scanning microscopy images of MDA-MB-231 cells 24 h after administration of TYE 563-
823 labelled siRNA-loaded BJExo. siRNA is labelled with TYE 563, nuclei is stained with DAPI (blue)
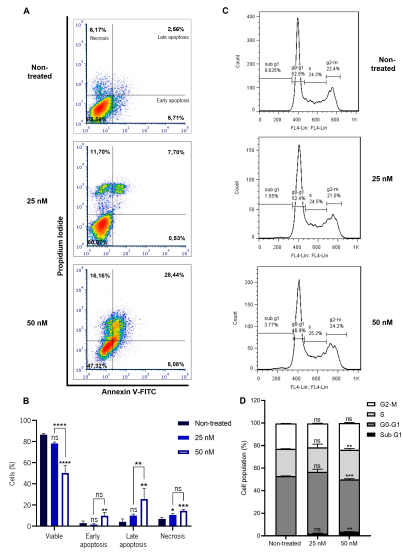824 and actin with Alexa fluor-488 phalloidin (green). Scale bar: 40 μm.

825 **Figure S3. Evaluation of silencing effect in PIK3CA levels**. Relative quantification of PIK3CA
826 mRNA levels in MDA-MB-231 and MDA-MB-453 cells treated with only exosomes (BJExo) or
827 loaded with siNC (BJExo[siNC]). Data are expressed as the fold change $\pm$ SD of three independent
828 experiments relative to the untreated condition after normalization to the reference gene (18S
829 rRNA). Two-way ANOVA indicates statistically significant differences within the group assessed
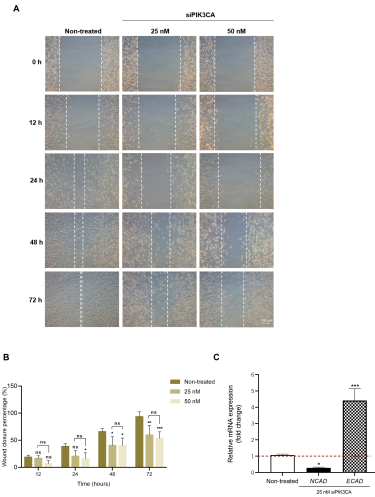830 by Sidak's post-test and denoted as follows: ns $p > 0.05$.

A

MDA-MB-231

B
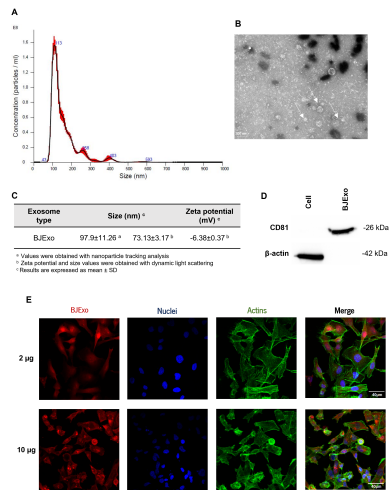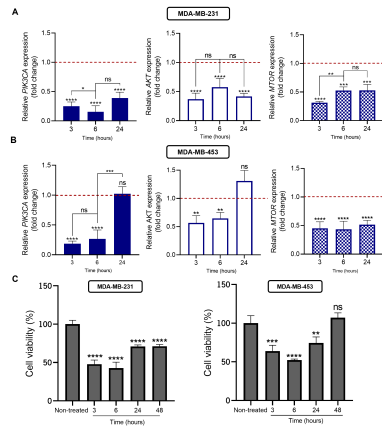
MDA-MB-453

A

B

C

A

B

C

Exosome type	Size (nm) [a]		Zeta potential (mV) [c]
BJExo	97.9±11.26 [a]	73.13±3.17 [b]	-6.38±0.37 [b]

[a] Values were obtained with nanoparticle tracking analysis
[b] Zeta potential and size values were obtained with dynamic light scattering
[c] Results are expressed as mean ± SD

D

CD81   -26 kDa

β-actin   -42 kDa

E

| BJExo | Nuclei | Actins | Merge |

2 µg

10 µg

A

MDA-MB-231

B

MDA-MB-453

C

MDA-MB-231

MDA-MB-453

- siPIK3CA affects the PAM pathway by downregulating mRNA and protein levels

- Impairment of the PAM pathway reduces breast cancer cells survival

- PIK3CA knockdown increases cellular apoptosis of MDA-MB-231 cells
- siPIK3CA delivered by exosomes promotes a faster and greater effect

Author Contributions: LR conceived and supervised the study. RS and DF performed the experiments, analyzed the data and wrote the manuscript. LR and DF gave suggestions on the experimental design. All authors reviewed the results and approved the final version of the manuscript.

Declaration of interests

☒ The authors declare that they have no known competing financial interests or personal relationships that could have appeared to influence the work reported in this paper.

☐ The authors declare the following financial interests/personal relationships which may be considered as potential competing interests: